THE ASTROPHYSICAL JOURNAL, 366:L5–L9, 1991 January 1

DUST AND GAS IN THE CORE OF ARP 220 (IC 4553)

N. Z. SCOVILLE,[1] A. I. SARGENT,[2] D. B. SANDERS,[3] AND B. T. SOIFER[2]
Division of Physics, Mathematics, and Astronomy, California Institute of Technology
Received 1990 July 19; accepted 1990 October 11

ABSTRACT

The CO and dust continuum emission in the ultraluminous infrared galaxy Arp 220 have been mapped at 1".9 × 2".1 resolution using the Owens Valley millimeter-wave interferometer. These aperture synthesis maps detect approximately 70% of the CO emission seen in single-dish measurements. Two emission components are identified—an extended component containing one-third of the flux and a compact, nuclear component containing $\frac{2}{3}$ of the flux. The extended component has a deconvolved size of 7".2 × 14".9, corresponding to 2.5 × 6.5 kpc; the major axis is approximately aligned with the optical dust lane. The nuclear source is resolved with a mean diameter of 1".7, corresponding to a radius of 315 pc. Velocity gradients with the same sense of rotation are seen in both components. The mass of gas (H_2 + He) in the central concentration is estimated to be $2.5 \times 10^{10}\ M_\odot$ (assuming a standard Galactic CO-to-H_2 conversion factor), yielding a mean H_2 density of 2900 cm^{-3} and surface density $8 \times 10^4\ M_\odot\ pc^{-2}$. The high extinction inferred from the gas surface densities ($A_V \sim 1000$ mag) can be reconciled with the detection of the nucleus at 2 μm if the central gas concentration is in a disk, inclined to the line-of-sight.

The continuum source at 2.7 mm is detected at a flux density of 30 mJy with an upper limit on the size of 1".5. The infrared/millimeter spectrum is well fitted by a source of size ~1".1 which is optically thick at $\lambda \lesssim 100$ μm.

These new data are analyzed together with those for the nuclei of other luminous *IRAS* galaxies. A correlation is found between the total luminosity-to-gas mass ratio and the central gas surface density. Thus, the high efficiency of energy production in these galaxies is linked to the high concentrations of interstellar matter, compatible with models in which the luminosity is generated by a nuclear starburst or a cental dust-embedded AGN. For Arp 220, the latter possibility is favored, since the 2.7 mm continuum flux limits the free-free emission at a level such that the starburst must be $\sim 10^9$ yr old or the initial mass function must be deficient at $\gtrsim 25\ M_\odot$.

Subject headings: galaxies: nuclei — interstellar: molecules

1. INTRODUCTION

The mechanisms proposed for the enormous luminosity in galaxies like Arp 220 include a burst of high-mass star formation (Joseph, Wright, & Wade 1984), a central nonthermal energy source (DePoy, Becklin, & Geballe 1987; Graham et al. 1990), or the kinetic energy of colliding galaxies (Harwitt et al. 1986). The interstellar matter may play a central role in all three scenarios—providing a dissipative medium for the galactic collision, promoting star formation, and fueling accretion onto a compact object (if such exists). Early aperture synthesis mapping in the 2.6 mm CO line showed approximately 70% of the total CO emission originating from an unresolved region <5" in size (corresponding to 1500 pc diameter) centered on the near-infrared nucleus (Scoville et al. 1986b). In this *Letter*, we report new higher sensitivity and higher angular resolution data for the CO emission and adjacent 2.7 mm continuum in Arp 220. The CO emission is resolved for the first time, and a kinematic gradient is detected parallel to the major axis of the optical dust lane.

[1] Postal address: Department of Astronomy, 105-24, California Institute of Technology, Pasadena, CA 91125.
[2] Postal address: Department of Physics, 320-47, California Institute of Technology, Pasadena, CA 91125.
[3] Postal address: Institute for Astronomy, University of Hawaii, 2680 Woodlawn Drive, Honolulu, HI 96822.

2. OBSERVATIONS

Arp 220 was observed using the Owens Valley Millimeter Interferometer between 1989 February and 1990 February. Nine configurations of the three telescopes were employed, the longest baseline being 200 m E-W. The synthesized beam size at $\lambda = 2.6$ mm was 1".9 × 2".1 (PA = 96°). Spectral resolution was provided by a 32 × 5 MHz filterbank, providing a total velocity coverage of 416 km s^{-1}, centered at $cz = 5486$ km s^{-1}. In addition, a contintuum channel with effective bandwidth of 375 MHz (975 km s^{-1}) was used for continuum and broad specral line measurements. Absolute flux calibration was based on observations of Uranus ($T_B = 120$ K) and 3C 273. For the resolution obtained here (1".9 × 2".1), $\Delta T_B = 1$ K corresponds to 43 mJy $beam^{-1}$. The rms noise in the 375 MHz continuum maps is 3.1 mJy $beam^{-1}$ in the lower sideband and 3.8 mJy $beam^{-1}$ in the upper sideband.

In Figure 1, the emission maps for the continuum channel in the lower (mostly dust emission) and upper sidebands (mostly CO emission) are shown as a function of displacement coordinates from the radio continuum peak ($\alpha_{1950} = 15^h32^m46^s.92$, $\delta_{1950} = 23°40'07".9$; Norris 1988). Both the CO and 110 Ghz continuum peak are within 0".5 of the brighter western component seen in the high-resolution near-infrared (Graham et al. 1990) and radio maps. The extended CO emission can best be seen in the emission maps with smaller velocity ranges (lower panels of Fig. 1). The low-level contours of CO emission are clearly extended along an NE-SW direction. It is also clear

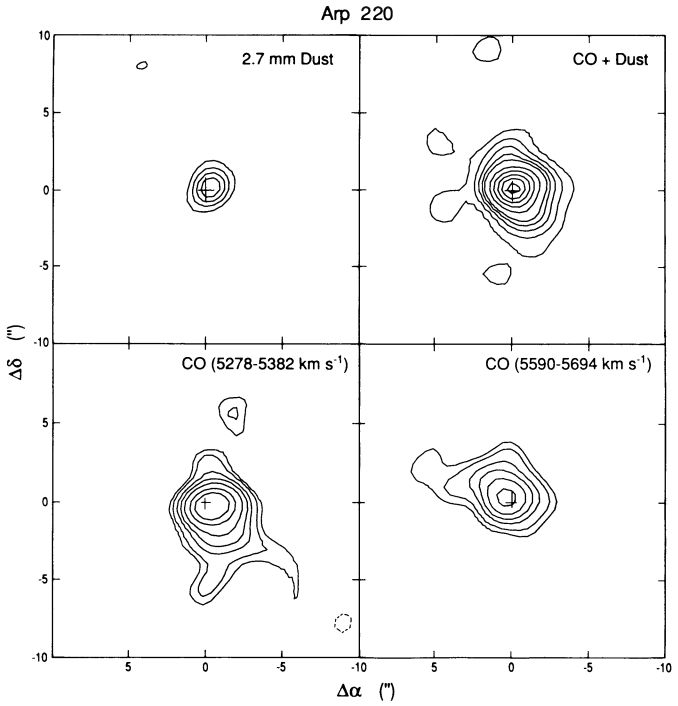

FIG. 1.—Emission observed in the continuum channel for the lower (mostly dust emission) and upper sidebands (the integrated CO emission plus a minor contribution from dust) are shown in the upper panels as a function of displacement coordinates from the centimeter-wave nonthermal radio peak (indicated by a plus sign) in Arp 220. Contours are at 8, 16, 24, 32, 40, 60, 80, 100, 120, and 140 mJy beam^{-1}. In the lower panels, the CO emission at 5278–5382 and 5590–5694 km s^{-1} are shown. Contours are at 3.1, 4.7, 7.8, 10.9, 15.6, 23.4, and 31.2 Jy km s^{-1} beam^{-1}. The synthesized beam is 1.″9 × 2.″1 (PA = 96°), and the rms noise is 3.8 mJy beam^{-1}. The peak broad-band flux (0.151 Jy beam^{-1}) corresponds to $\Delta T_B = 3.51$ K.

from these figures that there is a definite shift in the emission centroid as a function of velocity with lower velocities in the southwest and higher positive velocities in the northeast. Although the full velocity range of emission is seen in the central component, the emission spans a more limited velocity range in the displaced positions along the extended component.

In Table 1, the integrated fluxes and sizes are listed for a two-component fit to the integrated emission observed in the upper-sideband continuum filter containing the CO line (spanning 975 km s^{-1} centered at $cz = 5486$ km s^{-1}). In the lower sideband, 30 mJy is seen from an unresolved continuum source centered on the radio peak. This emission, attributed mostly to dust (see § 3.3), is presumably present in the upper sideband, and we have subtracted it from the upper sideband flux density of 424 mJy in order to estimate the total integrated CO emission (384 Jy km s^{-1}).

The residual CO emission can be separated into two components: a core 1.″4 × 1.″9 and an extended component 7″ × 5″ (deconvolved sizes). The former contains 67% of the flux detected by the interferometer; the latter contains the remaining 33%. Comparing the total CO line flux detected in the interferometer maps with that seen in single-dish measurements made with the IRAM 30 m telescope (Solomon, Radford, & Downes 1990), we estimate that these two components account for approximately 80% of the total CO emission from Arp 220. In the individual spectral line channels, the fraction of the single-dish flux detected is approximately 67% with no significant variation as a function of velocity over the observed 416 km s^{-1}. We therefore conclude that the higher velocity emission not included in the spectral line channels but included within the 375 MHz continuum channel has a higher visibility, and probably this emission is more concentrated in the core source.

3. DISCUSSION

3.1. *Molecular Gas*

In order to translate the observed CO line fluxes into molecular gas masses, we adopt a constant conversion factor based upon observations of Galactic GMCs (cf. Scoville & Sanders 1987). For $\alpha = 3 \times 10^{20}$ cm^{-2} (K km s^{-1})$^{-1}$, the H_2 mass is given by

$$M_{H_2} = 1.2 \times 10^4 S_{Jy} \Delta V d^2_{Mpc} , \quad (1)$$

where $S_{Jy}\Delta V$ is the integrated line flux. For standard interstellar abundances, the total gas mass is $1.36 M_{H_2}$. For the adopted distance of 77 Mpc, the total H_2 mass in Arp 220 is $3.5 \times 10^{10}\ M_\odot$, and the H_2 masses in the core and extended components are $1.8 \times 10^{10}\ M_\odot$ and $9 \times 10^9\ M_\odot$, respectively. The mean diameter of the core component ($\sim$1.″7) corresponds to a radius of 315 pc. The mean H_2 density, smoothed out over the volume, is 2900 cm^{-3}, and the averaged gas surface density (H_2 + He) is $8 \times 10^4\ M_\odot$ pc^{-2}.

The extraordinarily high mean gas density and possibly elevated gas temperatures which may exist in the nucleus of Arp 220 call into question the use of the standard Galactic CO-to-H_2 conversion factor. It is expected that the conversion ratio from the CO line flux to H_2 mass will scale approximately as $\rho^{1/2}/T_B$ (see Scoville & Sanders 1987). The peak flux density observed in the 5 MHz maps is 0.51 Jy beam^{-1} corresponding to a peak $\Delta T_B = 11.86$ K excess relative to the 2.75 K cosmic background. The true Planck brightness temperature is then 15 K. This suggests that the true *resolved* brightness temperatures in Arp 220 greatly exceed the typical 5–10 K bright-

TABLE 1

ARP 220 FLUX MEASUREMENTS

Measurements	Component	Flux	Deconvolved Size	PA
IRAM 30 m[a]	Total CO	480 Jy km s^{-1}	...	...
OVRO (LSB)	Dust (2.7 mm)	30 mJy	<1.″5	...
OVRO (USB)	CO + dust (2.7 mm)	424 mJy	...	...
OVRO (USB-LSB)	CO	384 Jy km s^{-1}	...	...
	Core component	257 Jy km s^{-1}	1.4 × 1.9	52°
	Extended component	127 Jy km s^{-1}	7 × 15	63

[a] Solomon, Radford, & Downes 1990.

ness temperatures observed for Galactic GMCs. Although the CO-to-H_2 conversion factor should then be reduced in Arp 220 due to the elevated gas temperatures, the higher gas densities will largely offset this effect.

3.2. *Kinematics and Dynamical Mass*

In Figure 1 (*lower panels*), a velocity gradient in both the core and extended components may be seen—the lower velocity emission shifted to the southwest of the nucleus and the higher velocity emission to the northeast. The direction of this velocity gradient is parallel to the major axes (PA = 52°–63°; Table 1) of the two CO emission components and to the dust lane seen prominently in optical photographs of Arp 220. Thus, the molecular gas in this merged galaxy system has partially relaxed to a disklike configuration with angular momentum playing a significant role in the gas distribution, inhibiting somewhat the further collapse toward the center.

Solomon, Radford, & Downes (1990) measure $\Delta V_{\rm FWZI} = 900$ km s^{-1} for the CO emission in Arp 220. If we assume that this full range of velocities exists within the central source of radius 315 pc, then the dynamical mass is $2.5 \times 10^{10}\ M_\odot$ for a spherical distribution. This dynamical mass is almost precisely equal to the total gas mass (H_2 + He) for the core component. Numerical simulations of merging galaxies which include a gas component show that due to its dissipative nature (Hernquist 1989), the gas sinks to the center of the merged system more readily than the stellar component and thus a high gas mass fraction is to be expected.

3.3. *Continuum*

In the lower sideband at 110.3 GHz, significant continuum emission was detected from the Arp 220 core source (30 ± 3 mJy; Table 1). This source was unresolved, placing an upper limit of 1".5 on the diameter. The radio nonthermal flux at $\lambda = 1.3$ cm is $\sim$36 mJy (Norris et al. 1985; Norris 1988), which extrapolates to a flux density of 11 mJy at 2.7 mm and to 7 mJy at 1.37 mm using a spectral index of -0.75 (Norris 1988). The residual emission (19 mJy at 2.7 mm) is probably dominated by the long-wavelength tail of the dust emission seen in the far-infrared, with a possible small contribution from free-free emission.

In Figure 2, the continuum flux densities between $\lambda = 2.7$ mm and 25 μm are plotted. These data include the observations reported here, as well as those of Woody et al. (1989), Eales, Wynn-Williams, & Duncan (1989), and the *IRAS* observations (cf. Soifer et al. 1990). To interpret these observations in terms of a thermal dust emission model, the $\lambda = 1.4$ and 2.7 mm observations were corrected for contributions from synchrotron emission as described above.

The data at $\lambda = 25$–100 μm are well fitted by a blackbody of temperature 64.7 K, while those at $\lambda = 60$ μm–2.7 mm are well-fitted by a single-temperature (42.2 K) grain model and an emissivity law $\epsilon \sim \lambda^{-1.3}$. If we assume that all of the observed emission comes from a single source, then the excellent fits to the data suggest that the source is becoming optically thick at $\lambda \sim 100$ μm. Then the size of a blackbody of 64.7 K that produces the 100 μm flux density, 1".13, represents a lower limit to the source size. This size is consistent with the observed limit on the source size at 2.7 mm. Comparison of the two models suggests that $\tau \sim 1$ occurs at $\lambda \sim 200$ μm; for a source of 1".13 diameter, this leads to a dust mass of $5 \times 10^7\ M_\odot$ for a mass opacity coefficient of 12 cm^2 gm^{-1} at 200 μm (e.g., Hildebrand 1983; Draine & Lee 1984). The implied gas-to-dust ratio is 400.

The $\lambda = 2.7$ mm continuum flux also provides a significant

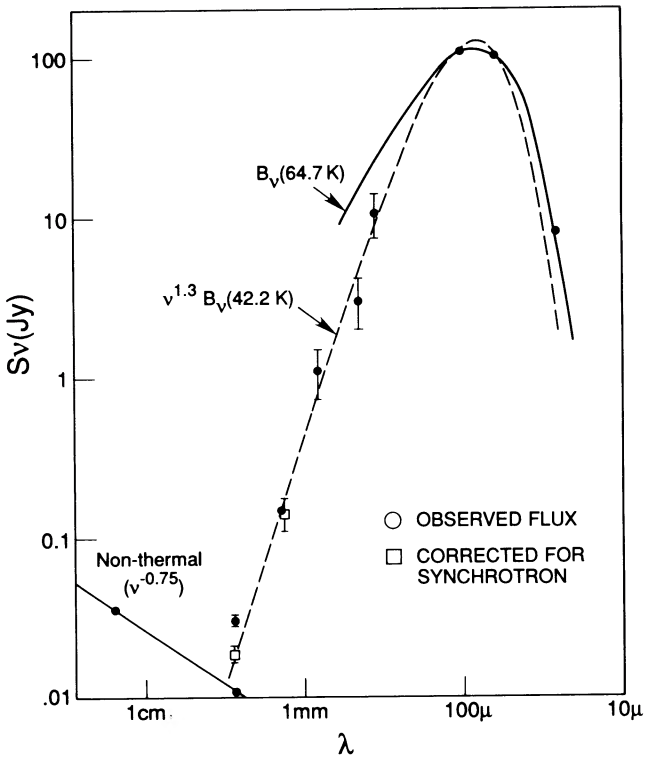

FIG. 2.—The continuum spectrum of Arp 220 is shown based on data (*solid points*) from this *Letter*, *IRAS*, Eales et al. (1989), Woody et al. (1989), and Norris (1988). The open square symbols are the millimeter wavelength fluxes corrected for synchrotron emission (Norris et al. 1985). The curves are blackbody and optically thin blackbody fits to the short- and long-wavelength data (see text).

constraint on the emission measure of ionized gas and thus the O star luminosity in the nucleus of Arp 220. For an optically thin plasma, the free-free flux density at 110 GHz is related to the ionizing photon production rate (Q_*) by

$$S_{110\ \rm GHz} = 8.4 \times 10^{-2}\ \frac{Q_*/10^{49}}{d^2_{\rm Mpc}}\ \rm mJy \qquad (2)$$

assuming that the H II regions are ionization-bounded and at a temperature of 10^4 K. If the maximum residual 2.7 mm flux after subtraction of the nonthermal and dust components is taken to be $\lesssim$10 mJy and it is assumed to be *entirely* free-free emission, then the upper limit for the emission rate of Lyman-continuum photons is 7.5×10^{54} s^{-1}. For an O5 star (60 $M_\odot$, $L = 5 \times 10^5\ L_\odot$), $Q_* = 4 \times 10^{49}$ s^{-1} and the ratio of the bolometric luminosity to the ionizing photon production rate is $1.9 \times 10^{-44}\ L_\odot$ s (Panagia 1973). The total luminosity corresponding to the derived upper limit to the ionizing photon production rate would be $10^{11}\ L_\odot$ for a population of O5 stars. Early O type stars by themselves would therefore fail to provide the observed far infrared luminosity in Arp 220 by a factor of at least 15. (Although a similar conclusion was reached by DePoy et al. [1987] on the basis of Brα measurements, there is some uncertainty regarding the near infrared extinction for Brα). For a mix of stellar masses, we may make use of the constant rate starburst models described by Scoville & Soifer (1990). With a modified Miller-Scalo initial mass function, their results may be parameterized by

$$\frac{L}{Q} = 1.2 \times 10^{-43}\left(\frac{t}{10^8\ \rm yr}\right)^{0.37}\left(\frac{m_u}{45}\right)^{\alpha} L_\odot\ \rm s^{-1}\ , \qquad (3)$$

where t is the age of the constant rate starburst, m_u is the upper mass cutoff for the IMF, and $\alpha = -1.54$ and -1.0 for $m_u < 45\ M_\odot$ and $m_u > 45\ M_\odot$. (Eq. [3] is accurate to $\sim 20\%$ for $t = 10^7$–5×10^8 yr, $m_u = 30$–$60\ M_\odot$.) For Arp 220, the *lower* limit on L/Q is $2.0 \times 10^{-43}\ L_\odot\ s^{-1}$. Comparing this with equation (3), we find that the duration of the burst must be $\sim 10^9$ yr for $m_u = 45\ M_\odot$ or $m_u \lesssim 20\ M_\odot$ for $t < 10^8$ yr. For $t = 10^8$ and 10^9 yr, the stellar masses required to produce the observed infrared luminosity are 2.9×10^{10} and $10^{12}\ M_\odot$ for an IMF with a lower limit of $0.1\ M_\odot$. The latter is clearly ruled out by the dynamical limit discussed in the preceding section. In summary, the low limit on the ionizing flux requires that the initial mass function of stars be severely truncated if the luminosity is to be provided by a starburst.

4. NUCLEAR GAS CONCENTRATIONS

Without exception, all of the infrared luminous galaxies for which high-resolution millimeter interferometer data have been obtained show evidence of significant dynamical perturbations, due to either a galactic interaction or a strong stellar bar, which could lead to concentration of the interstellar gas in the nuclear regions. In Table 2, we summarize the existing observational data for 18 of these galaxies observed with the Owens Valley millimeter-wave interferometer. In all cases, these galactic nuclei have far-infrared luminosity-to-molecular mass ratios significantly exceeding that of the Milky Way ($4\ L_\odot\ M_\odot^{-1}$; Scoville & Good 1989). This suggests that if the luminosity is generated by a population of young stars, the stars are either forming with a higher efficiency per unit mass of interstellar gas or with an initial mass function more heavily weighted toward high-mass, high-luminosity stars than that in the Milky Way. In the Galaxy, it has been suggested that high-mass star formation is triggered by the expansion of H II regions or supernova shells (e.g., Elmegreen and Lada 1977) or by cloud-cloud collisions (Scoville, Sanders, & Clemens 1986). Both processes depend on the *concentration* of molecular gas not merely its total mass.

In Figure 3, the total luminosity-to-mass ratios are shown as a function of central gas surface density ($M_\odot\ pc^{-2}$). In most cases, we have used the total infrared luminosities (since the *IRAS* resolution cannot separate the disk and nuclear contributions) and the *nuclear* gas masses in those galaxies for which actual size measurements have been obtained are plotted. The trend for increasing luminosity-to-mass ratios with increasing central gas surface densities is clear. These data thus strongly support the hypothesis that high efficiencies of energy generation seen in the infrared galaxy nuclei are related to the high central gas concentrations. The correlation found here is consistent with models in which high infrared luminosities are produced by populations of high-mass stars (formed via cloud-cloud collisions or stimulated processes) or those in which the luminosity is generated by accretion onto a compact, central black hole at a rate dependent on the ISM density. It is also consistent with the notion that some of the luminosity arises from dissipation of kinetic energy in the ISM.

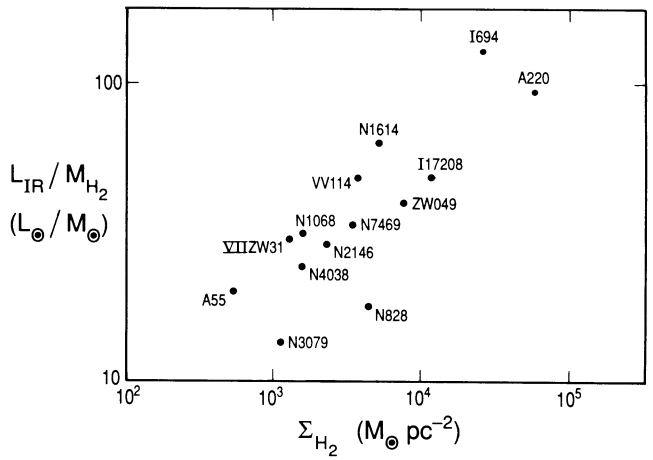

FIG. 3.—The infrared luminosity-to-molecular gas mass ratios are shown as a function of the central gas surface density for 14 luminous infrared galaxies for which high-resolution CO data have been obtained with the Owens Valley millimeter-wave interferometer. A general correlation is seen with increasing luminosity-to-mass ratios being found in the galaxies with higher gas surface densities.

This research was supported in part by NSF grant AST 87-14405.

TABLE 2

OVRO OBSERVATIONS OF HIGH-LUMINOSITY *IRAS* GALAXIES

Object	$\langle cz \rangle$ (km s^{-1})	D (Mpc)	Radius (arcsec) (kpc)	L_{IR} ($10^{11}\ L_\odot$)	Nuclear M_{H_2} ($10^9\ M_\odot$)	M_{H_2}/M_{dyn}	CO Morphology	References
Mrk 231	12660	174	<3.5 (2.9)	34.7	36.0	...	100% nuclear source	1
IRAS 1708−0014	12850	175	1.5 (1.3)	27.0	55.0	...	100% nuclear source	2
Arp 220	5452	77	1 (0.3)	15.5	16.3	0.90	70% nuclear source	
VII Zw 31	16245	221	2.5 (2.7)	8.7	29.4	...	60% nuclear source	1
IRAS 10173+028	14680	196	3.5 (3.3)	6.0	9.0	...	40% nuclear source	2
NGC 6240	7285	101	3.5 (1.7)	6.6	11.2	0.77	Interacting pair	3
IC 694 (Arp 299)	3060	42	1.2 (0.3)	4.9	3.9	...	Triple source	4
VV 114	6028	78	2.5 (0.9)	4.2	10.0	...	Double source	1
NGC 1614	4847	62	2 (0.6)	4.0	6.0	...	30% nuclear source	1
Arp 55	11957	163	4 (3.2)	3.9	17.3	0.6	Double source	5
NGC 1068	1137	18	1.5 (0.13)	1.5	4.5	...	Ring + nuclear source	6
NGC 7469 (Arp 298)	4963	66	2.5 (0.8)	2.6	7.4	0.7	30% nuclear source	5
Zw 049.057	3900	52	1.4 (0.4)	1.7	4.6	...	40% nuclear source	2
NGC 828	5359	72	2.5 (0.9)	2.1	11.8	0.31	Interacting pair	5
NGC 2146	838	21	4/13 (0.4)	1.2	4	...	...	7
NGC 3079	1137	24	3/7 (0.3)	0.7	5	0.2	...	8
NGC 520 (Arp 157)	2261	29	2.5 (0.4)	0.6	3.2	...	Interacting pair	5
NGC 4038/39 (Arp 244)	1550	21	3.5 (0.4)	0.2	0.8	...	Triple source	9

REFERENCES.—(1) Scoville et al. 1989; (2) Planesas, Mirabel, & Sanders 1991; (3) Wang, Scoville, & Sanders 1991; (4) Sargent & Scoville 1991; (5) Sanders et al. 1988a; (6) Planesas, Scoville, & Myers 1991; (7) Young, Claussen, & Scoville 1988; (8) Young et al. 1988; (9) Stanford et al. 1990.

REFERENCES

DePoy, D. L., Becklin, E. E., & Geballe, T. R. 1987, ApJ, 316, L63
Draine, B., & Lee, H. M. 1984, ApJ, 285, 89
Eales, S. A., Wynn-Williams, C. G., & Duncan, W. D. 1989, ApJ, 339, 859
Elmegreen, B. G., & Lada, C. J. 1977, ApJ, 214, 725
Graham, J. R., Carico, D. P., Matthews, K., Neugebauer, G., Soifer, B. T., & Wilson, T. D. 1990, ApJ, 354, L5
Harwit, M., Houck, J. R., Soifer, B. T., & Palumbo, G. G. C. 1986, ApJ, 315, 28
Hernquist, L. 1989, Nature, 340, 687
Hildebrand, R. H. 1983, QJRAS, 24, 267
Joseph, R. D., Wright, G. S., & Wade, R. 1984, Nature, 311, 132
Norris, R. P. 1988, MNRAS, 230, 345
Norris, R. P., Bean, W. A., Haschick, A. D., Booth, R. S., & Diamond, P. J. 1985, MNRAS, 213, 821
Panagia, N. 1973, AJ, 78, 929
Planesas, P., Mirabel, I. F., & Sanders, D. B. 1991, ApJ, in press
Planesas, P., Scoville, N. Z., & Myers, S. T. 1991, ApJ, in press
Sanders, D. B., Scoville, N. Z., Sargent, A. I., & Soifer, B. T. 1988a, ApJ, 324, L55
Sanders, D. B., Soifer, B. T., Elias, J. H., Madore, B. F., Matthews, K., Neugebauer, G., & Scoville, N. Z. 1988b, ApJ, 325, 74
Sargent, A. I., & Scoville, N. Z. 1991, in preparation
Scoville, N. Z., & Good, J. C. 1989, ApJ, 339, 149
Scoville, N. Z., & Sanders, D. B. 1987, in Interstellar Processes, ed. D. J. Hollenbach and H. A. Thronson (Dordrecht: Reidel), p. 21
Scoville, N. Z., Sanders, D. B., & Clemens, D. P. 1986a, ApJ, 310, L77
Scoville, N. Z., Sanders, D. B., Sargent, A. I., Soifer, B. T., Scott, S. L., & Lo, K. Y. 1986b, ApJ, 311, L47
Scoville, N. Z., Sanders, D. B., Sargent, A. I., Soifer, B. T., & Tinney, C. G. 1989, ApJ, 345, L25
Scoville, N. Z., & Soifer, B. T. 1990, in Massive Stars and Starbursts, ed. K. Leitherer (Cambridge: Cambridge University Press), in press
Soifer, B. T., et al. 1990, ApJ, in press
Solomon, P. M., Radford, S. J. E., & Downes, D. 1990, ApJ, 348, L53
Stanford, S. A., Sargent, A. I., Sanders, D. B., & Scoville, N. Z. 1990, ApJ, 349, 492
Wang, Z., Scoville, N. Z., & Sanders, D. B. 1991, ApJ, in press
Woody, D. P., Scott, S. L., Scoville, N. Z., Mundy, L. G., Sargent, A. I., Padin, S., Tinney, C. G., & Wilson, C. D. 1989, ApJ, 337, L41
Young, J. S., Claussen, M. J., Kleinmann, S. G., Rubin, V. C., & Scoville, N. Z. 1988, ApJ, 331, L81
Young, J. S., Claussen, M. J., & Scoville, N. Z. 1988, ApJ, 324, 115